Journal of Porphyrins and Phthalocyanines
J. Porphyrins Phthalocyanines 2013; **17**: 1–13
DOI: 10.1142/S1088424613500612

Published at http://www.worldscinet.com/jpp/

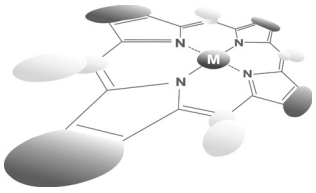

β-Nitro-substituted free-base, iron(III) and manganese(III) tetraarylporphyrins: synthesis, electrochemistry and effect of the NO_2 substituent on spectra and redox potentials in non-aqueous media

Shuibo Yang[a], Bin Sun[a], Zhongping Ou*[a◊], Deying Meng[a], Guifen Lu[a◊◊], Yuanyuan Fang[b] and Karl M. Kadish*[b◊]

[a] *School of Chemistry and Chemical Engineering, Jiangsu University, Zhenjiang 212013, P. R. China*
[b] *Department of Chemistry, University of Houston, Houston, TX 77204-5003, USA*

Dedicated to Professor Evgeny Luk'yanets on the occasion of his 75th birthday

Received 21 March 2013
Accepted 18 April 2013

ABSTRACT: Two free-base and four metal derivatives of substituted tetraarylporphyrins containing a nitro-substituent on the β-pyrrole position of the macrocycle were synthesized and characterized by UV-vis, FTIR, ^{1}H NMR and mass spectrometry as well as electrochemistry and spectroelectrochemistry in non-aqueous media. The porphyrins are represented as (NO_2TmPP)M and (NO_2TdmPP)M, where M = 2H, $Fe^{III}Cl$ or $Mn^{III}Cl$, m is a CH_3 group on the *para*-position of the four *meso*-phenyl rings of the tetraphenylporphyrin (TPP) and dm represents two OCH_3 substituents on the meta-positions of each phenyl ring of the TPP macrocycle. UV-visible spectra of the nitro-substituted porphyrins exhibit absorption bands which are red-shifted by 4–11 nm as compared to bands of the same substituted tetraarylporphyrins lacking a nitro substituent. Three or four reductions are observed for each iron and manganese nitroporphyrin, the first of which is metal-centered, leading to formation of an Fe(II) or Mn(II) complex. Further reduction at the metal center occurs for the iron porphyrins but this reaction proceeds *via* an Fe(II) π anion radical in the case of the two nitro-substituented derivatives. The β-nitro-substituted porphyrins are easier to reduce and harder to oxidize than the corresponding compounds lacking a nitro group. The effect of NO_2 substituent on reduction/oxidation potentials and the site of electron transfer was also discussed.

KEYWORDS: iron and manganese porphyrins, β-nitro-substituent, synthesis, electrochemistry, effect of substituent.

INTRODUCTION

Metalloporphyrins and their analogues have attracted considerable attention for use in a broad range of applications [1–3] because of their versatile properties derived from the characteristic π-ring system and coordinating ability of the central metal ion. There are many ways to "tune" or change the properties of a porphyrin, the most common of which involves changes in the peripheral functionalization, *i.e.* introducing electron-withdrawing or electron-donating substituents onto the meso and/or β-pyrrole positions of the macrocycle.

The addition of one or more highly electron-withdrawing NO_2 groups to a porphyrin will significantly modify its chemical and physical properties, with the type and magnitude of the effect being dependent in large part on the position of the substituents. Four types of nitro-substituted porphyrins have been extensively examined in the last

◊SPP full and ◊◊ student member in good standing

*Correspondence to: Zhongping Ou, email: zpou2003@yahoo.com, tel/fax: +86 511-8879-1800; Karl M. Kadish, email: kkadish@uh.edu, tel: +1 (713)-743-2740, fax: +1 (713)-743-2745

three decades [4–52]. These are: (i) *meso*-NO_2 substituted octaethylporphyrins [36–40], (ii) β-pyrrole substituted porphyrins [4–35], (iii) *meso*-phenyl substituted derivatives [41–47] and (iv) porphyrins containing one or more NO_2 substituents on a β,β′-fused group(s) of the macrocycle as in the case of nitro-substituted quinoxalinoporphyrins [48–51].

Previous electrochemical characterization of nitroporphyrins with redox inactive central metal ions have shown that the presence of one or more electron-withdrawing NO_2 groups at the *meso*- or β-pyrrole positions of the conjugated macrocycle will have a large effect on the $E_{1/2}$ for electroreduction, shifting the reversible potentials in a positive direction by 230–380 mV per nitro group in the case of β-pyrrole substituted (TPP)M and by 450–550 mV in the case of *meso*-substituted (OEP)M type derivatives [52]. The NO_2 group on the phenyl ring of a TPP type complex [52, 53] or the quinoxaline group of a quinoxalinoporphyrin [51] may itself be involved in an electroreduction. However, a direct reduction of the NO_2 group does not occur in non-aqueous media when this electron-withdrawing group is attached at the *meso* or β-pyrrole position of the porphyrin ring and the main effect is to shift $E_{1/2}$ for the oxidation and reduction. In a few cases, the addition of NO_2 to the porphyrin macrocycle has been shown to change the site of electron transfer from metal to macrocycle, one example being given in the case of β-pyrrole substituted [(NO_2)P]$Au^{III}PF_6$ [31], where P = 5,10,15,20-tetrakis(3,5-di-*tert*-butylphenyl)porphyrin. Finally, it should be pointed out that NO_2 substitution at the β-pyrrole or *meso*-position of a porphyrin ring has a much smaller effect on $E_{1/2}$ for oxidation than for reduction, and this has been well-documented in the literature for a variety of TPP and OEP type complexes [52].

In the present work, six β-pyrrole nitro-substituted porphyrins with redox active central metal ions were synthesized and characterized as to their electrochemical and spectroelectrochemical properties in non-aqueous media. The investigated compounds are represented as (NO_2TmPP)M and (NO_2TdmPP)M, where M = 2H, $Fe^{III}Cl$ or $Mn^{III}Cl$, m is a CH_3 group located at the para-position of the four *meso*-phenyl rings and dm represents two OCH_3 substituents located at the 3,5 (meta)-positions of the phenyl rings of the TPP macrocycle (Chart 1). The effect of the β-nitro group on the UV-visible spectra and

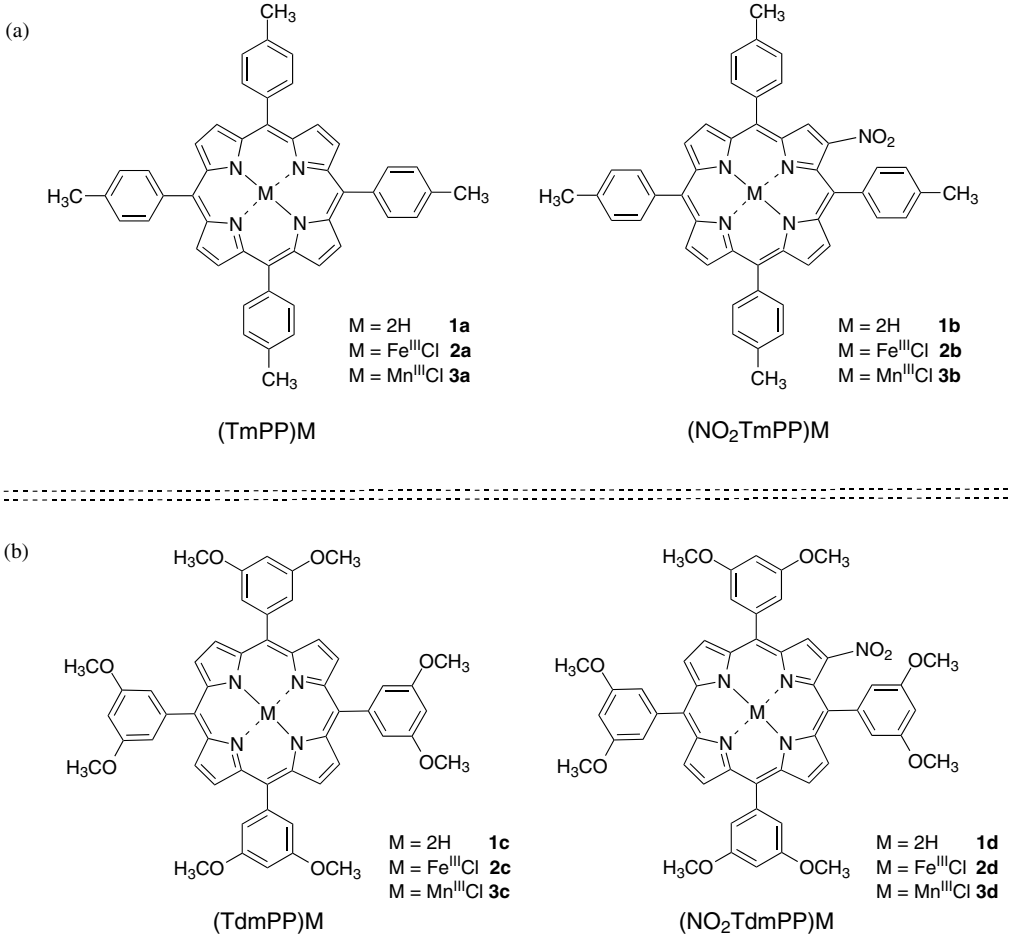

Chart 1. Structures of tetraarylporphyrins and β-NO_2 substituted tetraarylporphyrins

reduction/oxidation potentials is discussed in terms of comparisons with the non-nitro substituted porphyrins having the same central metal ions. Comparisons are also made to previously investigated porphyrins and β-nitro substituted corroles, both the free-base derivatives [54] and corroles containing transition metal ions such as iron [55], copper [56], germanium [56] and silver [57].

EXPERIMENTAL

Materials and instrumentation

Reagents and solvents (Sigma-Aldrich, Fluka or Sinopharm Chemical Reagent Co.) for synthesis and purification were of analytical grade and used as received. Dichloromethane (CH_2Cl_2, 99.8%) was purchased from Sinopharm Chemical Reagent Co. and fresh distilled before use. Tetra-*n*-butylammonium perchlorate (TBAP) was purchased from Sigma Chemical or Fluka Chemika Co., recrystallized from ethyl alcohol, and dried under vacuum at 40 °C for at least one week prior to use.

^{1}H NMR spectra were recorded in a $CDCl_3$ solution at 400 MHz using a Bruker Advance 400 spectrometer at 25 °C. Chemical shifts (ppm) were determined with TMS as the internal reference. MALDI-TOF mass spectra were carried out on a Bruker BIFLEX III ultrahigh resolution.

Cyclic voltammetry was carried out at 298 K using a CHI-730C Electrochemical Workstation. A homemade three-electrode cell was used for cyclic voltammetric measurements and consisted of a glassy carbon working electrode, a platinum counter electrode and a homemade saturated calomel reference electrode (SCE). The SCE was separated from the bulk of the solution by a fritted glass bridge of low porosity which contained the solvent/supporting electrolyte mixture.

Thin-layer UV-visible spectroelectrochemical experiments were performed with a home-built thin-layer cell which has a light transparent platinum net working electrode. Potentials were applied and monitored with a CHI-730C Electrochemical Workstation. Time-resolved UV-visible spectra were recorded with a Hewlett-Packard Model 8453 diode array spectrophotometer. High purity N_2 was used to deoxygenate the solution and a stream of nitrogen gas was kept over the solution during each electrochemical and spectroelectrochemical experiment.

Synthesis

5,10,15,20-Tetrakis(3,5-dimethoxyphenyl)-porphyrin, (TdmPP)H_2 1c. (TdmPP)H_2 was synthesized by the reaction of pyrrole and 3,5-dimethoxybenzaldehyde according to a procedure in the literature [58]. UV-vis (CH_2Cl_2): λ_{max}, nm 420, 514, 549, 589, 644. ^{1}H NMR (400 MHz, $CDCl_3$): δ_H, ppm 8.93 (s, 8H, pyrrole-*H*), 7.4 (s, 8H, ph-*H*), 6.9 (s, 4H, ph-*H*), 3.96 (s, 24H, -OCH_3), -2.83 (s, 2H, pyrrole-N*H*). MS (MALDI-TOF): *m/z* 856.85 (calcd. for $[M + 2H]^+$ 855.95).

2-Nitro-5,10,15,20-tetrakis(3,5-dimethoxyphenyl)-porphyrin copper(II), (NO_2TdmPP)Cu. A mixture of (TdmPP)H_2 (320 mg, 0.375 mmol), copper(II) acetate monohydrate (460 mg, 2.304 mmol), chloroform (120 mL), glacial acetic acid (3 mL) and methanol (3 mL) was heated at 50–60 °C for 3 h until the (TdmPP)H_2 was not detected by silica TLC. After that, copper nitrate trihydrate (214 mg, 0.885 mmol) and acetic anhydride (7 mL) was then poured into the mixture, and, continue to stir for 2.5 h at 40–50 °C. The reaction mixture was allowed to cool and washed with water, ammonia, water, dried over anhydrous $MgSO_4$. The residue was passed through a plug of alumina using dichloromethane as eluent. The main fraction was collected and the solvent completely removed to give a red-purple solid (300 mg, yield 83%). UV-vis (CH_2Cl_2): λ_{max}, nm 427, 548, 591. MS (MALDI-TOF): *m/z* 961.34 (calcd. for $[M + 2H]^+$ 961.24).

2-Nitro-5,10,15,20-tetrakis(3,5-dimethoxyphenyl)-porphyrin, (NO_2TdmPP)H_2 1d. (NO_2TdmPP)Cu (200 mg, 0.208 mmol) was slowly added to a concentrated sulfuric acid (15 M, 4 mL) and stirred vigorously. After 15 min of stirring, the reaction mixture was neutralized with ammonia and extracted with chloroform. The extract was dried over sodium sulfate and evaporated to dryness. The residue was dissolved in dichloromethane and eluted with the same solvent through a column of alumina. The major eluted fraction was again evaporated to dryness and afforded a purple solid (NO_2TdmPP)H_2 (140 mg, yield 75%). UV-vis (CH_2Cl_2): λ_{max}, nm 432, 528, 597, 668. ^{1}H NMR (400 MHz, $CDCl_3$): δ_H, ppm 9.18 (s, 2H, pyrrole-*H*), 9.02–9.05 (d, 3H, pyrrole-*H*), 8.83 (s, 2H, pyrrole-*H*), 7.39–7.46 (m, 8H, ph-*H*), 6.91–6.93 (m, 4H, ph–*H*), 4.0 (s, 24H, -OCH_3), -2.67 (s, 2H, pyrrole-N*H*). MS (MALDI-TOF): *m/z* 901.24 (calcd. for $[M + 2H]^+$ 900.95).

2-Nitro-5,10,15,20-tetrakis(*p*-methylphenyl)porphyrin(NO_2TmPP)H_2 1b. The synthesis of (NO_2TmPP)H_2 was carried out as described for (NO_2TdmPP)H_2. UV-vis (CH_2Cl_2): λ_{max}, nm 426, 530, 601, 668. ^{1}H NMR (400 MHz, $CDCl_3$): δ_H, ppm 8.76–9.09 (m, 7H, pyrrole-*H*) 8.09–8.18 (m, 8H, ph-*H*), 7.54–7.60 (m, 8H, ph-*H*), 2.70–2.73 (m, 12H, -CH_3), -2.57 (s, 2H, pyrrole-N*H*). MS (MALDI-TOF): *m/z* 717.01 (calcd. for $[M + 2H]^+$ 716.85).

Iron(III) and manganese(III) porphyrins were synthesized by reaction of the corresponding free-base porphyrin and a metal salt according to the route shown in Scheme 1.

(TmPP)FeCl 2a. Yield 87%. UV-vis (CH_2Cl_2): λ_{max}, nm 386, 418, 512. IR (KBr): ν, cm^{-1} 998 ($\nu_{N\text{-}Fe}$). MS (MALDI-TOF): *m/z* 726.23 (calcd. for $[M - Cl + 2H]^+$ 726.68).

(NO_2TmPP)FeCl 2b. Yield 62%. UV-vis (CH_2Cl_2): λ_{max}, nm 382, 428, 518. IR (KBr): ν, cm^{-1} 1525, 1331 (ν_{NO2}), 999 ($\nu_{N\text{-}Fe}$). MS (MALDI-TOF): *m/z* 770.99 (calcd. for $[M - Cl + 2H]^+$ 771.68).

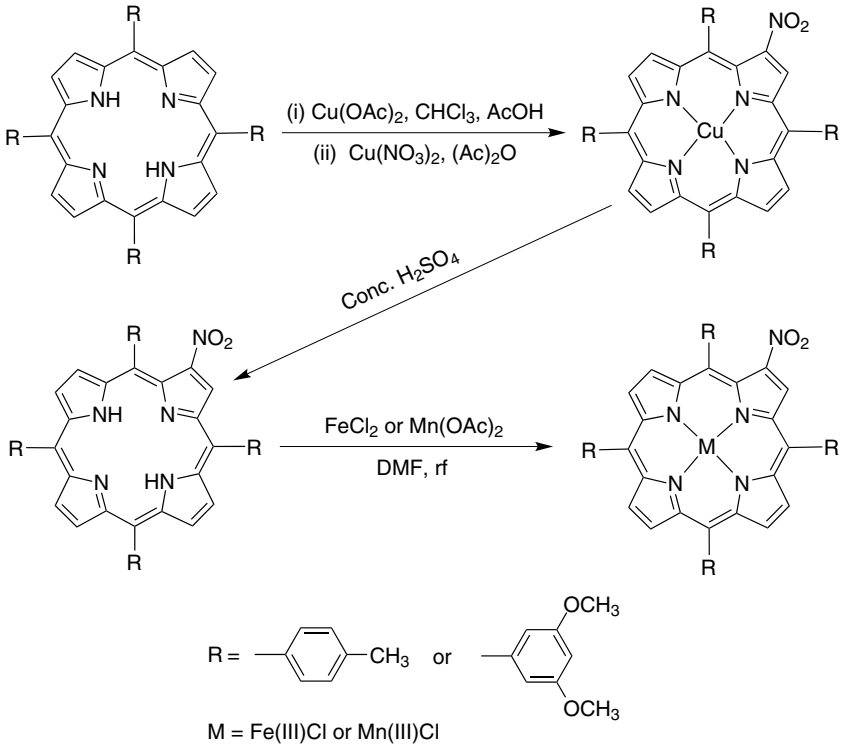

Scheme 1. Synthesis routes of the β-nitro-substituted porphyrins

(TdmPP)FeCl 2c. Yield 85%. UV-vis (CH_2Cl_2): λ_{max}, nm 370, 422, 511. IR (KBr): ν, cm^{-1} 1001($\nu_{N\text{-}Fe}$). MS (MALDI-TOF): *m/z* 910.03 (calcd. for $[M - Cl + 2H]^+$ 910.79).

(NO_2TdmPP)FeCl 2d. Yield 65%. UV-vis (CH_2Cl_2): λ_{max}, nm 374, 433, 521. IR (KBr): ν, cm^{-1} 1522, 1348 (ν_{NO2}), 1006 ($\nu_{N\text{-}Fe}$). MS (MALDI-TOF): *m/z* 955.15 (calcd. for $[M - Cl + 2H]^+$ 955.78).

(TmPP)MnCl 3a. Yield 89%. UV-vis (CH_2Cl_2): λ_{max}, nm 379, 480, 622. IR (KBr): ν, cm^{-1} 1008 ($\nu_{N\text{-}Mn}$). MS (MALDI-TOF): *m/z* 725.12 (calcd. for $[M - Cl + 2H]^+$ 725.78).

(NO_2TmPP)MnCl 3b. Yield 81%. UV-vis (CH_2Cl_2): λ_{max}, nm 382, 484, 630. IR (KBr): ν, cm^{-1} 1524, 1338 (ν_{NO2}), 1009 ($\nu_{N\text{-}Mn}$). MS (MALDI-TOF): *m/z* 769.99 (calcd. for $[M - Cl + 2H]^+$ 770.77).

(TdmPP)MnCl 3c. Yield 82%. UV-vis (CH_2Cl_2): λ_{max}, nm 380, 481, 615. IR (KBr): ν, cm^{-1} 1024 ($\nu_{N\text{-}Mn}$). MS (MALDI-TOF): *m/z* 909.15 (calcd. for $[M - Cl + 2H]^+$ 909.88).

(NO_2TdmPP)MnCl 3d. Yield 51%. UV-vis (CH_2Cl_2): λ_{max}, nm 384, 490, 623. IR (KBr): ν, cm^{-1} 1525, 1349 (ν_{NO2}), 1026 ($\nu_{N\text{-}Mn}$). MS (MALDI-TOF): *m/z* 954.22 (calcd. for $[M - Cl + 2H]^+$ 954.88).

RESULTS AND DISCUSSION

Synthesis

To the first step, the $(TRPP)H_2$ was treated with copper(II) acetate in chloroform to produce (TRPP)Cu. The copper porphyrins were not separated from the solution and used directly for the following nitration step to synthesis of (NO_2TRPP)Cu [58]. The β-pyrrole NO_2 substituted copper porphyrins were purified by a plug of alumina using dichloromethane as eluent and demetalated in concentrated sulfuric acid to give the corresponding β-pyrrole NO_2 substituted free-base porphyrins. The (NO_2TRPP)M complexes (M = FeCl or MnCl) were then synthesized *via* a reaction between the free-base nitroporphyrin (NO_2TRPP)H_2 and the corresponding metal salt in DMF (see Scheme 1). The purity of the final synthesized porphyrins was confirmed by ^{1}H NMR, UV-vis spectroscopy and mass spectrometry.

UV-visible spectra

UV-visible spectra of the porphyrins were measured in CH_2Cl_2. The λ_{max} values of each compound are summarized in Table 1 and examples of UV-visible spectra for the TmPP and TdmPP derivatives are illustrated in Fig. 1. As seen in the figure and table, the Soret bands of $(TmPP)H_2$ **1a** and $(TdmPP)H_2$ **1c**, (TmPP)FeCl **2a** and (TdmPP)FeCl **2c** or (TmPP)MnCl **3a** and (TdmPP)MnCl **3c** are located at almost identical values of λ_{max}. This result indicates that changing substituents on the four meso-phenyl rings of the porphyrin from one para-CH_3 group to two OCH_3 substituents at the meta-positions of the phenyl ring has only a negligible effect on UV-visible spectra.

In contrast, significant differences are seen between UV-visible spectra of the NO_2 substituted porphyrins

Table 1. UV-visible spectral data (λ_{max}, nm) of the neutral and reduced porphyrins in CH_2Cl_2, 0.1 M TBAP

M	Compound	β-sub	*meso*-sub[a]	Soret region		Visible region			
2H	**1a**	H	CH_3	419		515	552	590	651
	1b	NO_2	CH_3	426		530	601	668	
	1c	H	OCH_3	420		514	549	589	644
	1d	NO_2	OCH_3	432		528	597	668	
Fe(III)	**2a**	H	CH_3	386	418	512			
	2b	NO_2	CH_3	382	428	518			
	2c	H	OCH_3	370	422	511			
	2d	NO_2	OCH_3	374	433	521			
Mn(III)	**3a**	H	CH_3	379	480	582	622		
	3b	NO_2	CH_3	382	484	586	630		
	3c	H	OCH_3	378	481	581	616		
	3d	NO_2	OCH_3	390	490	594	640		
Fe(II)	**[2a]**$^-$	H	CH_3	418	445	540			
	[2b]$^-$	NO_2	CH_3	428	444	541			
	[2c]$^-$	H	OCH_3	420	445	540			
	[2d]$^-$	NO_2	OCH_3	433	446	544			
Mn(II)	**[3a]**$^-$	H	CH_3	403	445	578	619		
	[3b]$^-$	NO_2	CH_3	408	450	590	650		
	[3c]$^-$	H	OCH_3	404	446	576	616		
	[3d]$^-$	NO_2	OCH_3	410	457	590	635		
Fe(I)[b]	**[2a]**$^{2-}$	H	CH_3	417	443	577	618		
	[2b]$^{2-}$	NO_2	CH_3	420	444	541	616	690	
	[2c]$^{2-}$	H	OCH_3	420	445	570	614		
	[2d]$^{2-}$	NO_2	OCH_3	426	446	544	620	695	

[a] Substituents on the *meso*-phenyl rings of the porphyrin macrocycle. [b] Fe(II) π-anion radical is the major product upon the second reduction of the β-NO_2 substituted compound.

and their unsubstituted parent compounds. The Soret bands of the nitro-porphyrins are broader and red-shifted by 4–11 nm as compared to λ_{max} of the unsubstituted compounds. The largest red-shift ($\Delta\lambda$ = 11 nm) is seen upon going from (TdmPP)H_2 **1c** to (NO_2TdmPP)H_2 **1d** and the smallest ($\Delta\lambda$ = 4 nm) upon going from (TmPP)MnCl **3a** to (NO_2TmPP)MnCl **3b**.

Electrochemistry

The unsubsituted and nitro-substituted TmPP and TdmPP complexes were examined as to their electrochemistry and spectroelectrochemistry in CH_2Cl_2 containing 0.1 M TBAP. A summary of the measured half-wave and peak potentials for each redox process is given in Table 2.

Free-base porphyrins. Each currently examined free-base porphyrin undergoes two reversible one-electron reductions and two reversible one-electron oxidations in CH_2Cl_2 containing 0.1 M TBAP. The NO_2 group on the two nitroporphyrins is not reduced, consistent with what occurs for other β-pyrrole NO_2 substituted porphyrins [23]. However, as expected, half-wave potentials of the free-base nitroporphyrins are shifted positively by 110–130 mV for the first oxidation and by 280–290 mV for the first reduction, as compared to $E_{1/2}$ values of the parent porphyrins lacking an NO_2 group (Table 2). Similar behavior was reported for the oxidation and reduction of (TPP)H_2 and (NO_2TPP)H_2 [23].

Iron porphyrins. The two non-nitro iron porphyrins (**2a** and **2c**) undergo three one-electron reductions in CH_2Cl_2 containing 0.1 M TBAP while four reductions are observed for the two nitro-substituted Fe(III) compounds (**2b** and **2d**) under the same solution conditions. In addition, the nitro-substituted Fe(III) porphyrins are easier to reduce and harder to oxidize than the unsubstituted TmPP or TdmPP Fe(III) complexes. For example, the first two reductions and two oxidations of (NO_2TdmPP)FeCl **2d** in CH_2Cl_2 are located at $E_{1/2}$ = -0.16, -0.79 V. 1.23 and 1.41 V as compared to the corrosponding redox of

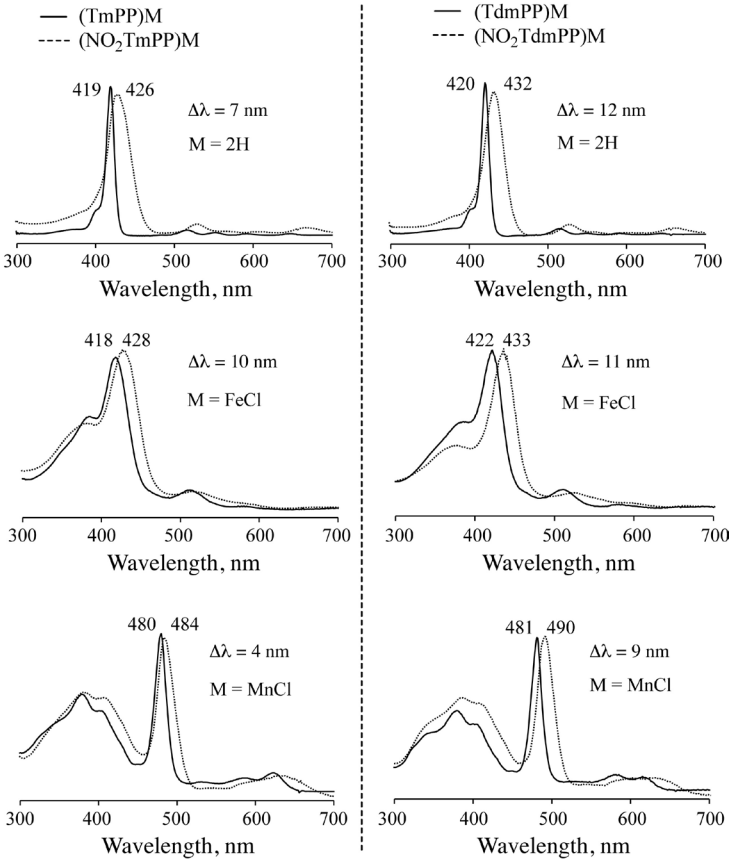

Fig. 1. Comparisons between UV-visible spectra of β-NO_2 substituted porphyrins (-------) and porphyrins without NO_2 group (——), Δλ is the difference in wavelength of the Soret bands between the two types of porphyrins

Table 2. Half-wave potentials (V *vs.* SCE) of porphyrins in CH_2Cl_2 containing 0.1 M TBAP

M	Compound	β-sub	*meso*-sub[a]	Ring-oxidation		M^{III}/M^{II}	Ring-reduction[b]	
				2nd	1st		1st	2nd
2H	**1a**	H	CH_3	1.15	0.95		-1.19	-1.70[c]
	1b	NO_2	CH_3	1.25	1.06		-0.81	-1.60[c]
	1c	H	OCH_3	1.24	1.02		-1.12	-1.60[c]
	1d	NO_2	OCH_3	1.44	1.15		-0.83	-1.57
Fe(III)	**2a**	H	CH_3	1.35	1.07	-0.27	-1.04	-1.71[c]
	2b	NO_2	CH_3	1.38	1.14	-0.18	-0.81[d]	-1.29[c]
	2c	H	OCH_3	1.32	1.14	-0.28	-1.01	-1.71[c]
	2d	NO_2	OCH_3	1.41	1.23	-0.16	-0.79[d]	-1.31[c]
Mn(III)	**3a**	H	CH_3	1.42	1.08	-0.31	-1.62[c]	
	3b	NO_2	CH_3	1.56	1.18	-0.15	-1.14	-1.73[c]
	3c	H	OCH_3	1.48	1.14	-0.29	-1.60[c]	
	3d	NO_2	OCH_3	1.50	1.26	-0.10	-1.10	-1.66[c]

[a] Substituents on the four phenyl rings of porphyrin macrocycle (see Chart 1). [b] The second reduction of the Fe(III) porphyrin was metal-centered electron transfer process for **2a** and **2c**. [c] Irreversible peak potential at a scan rate of 0.1 V/s. [d] Additional reduction observed at E_{pc} = -1.13 (**2b**) and -0.99 V (**2d**) (see Fig. 2 and discussion in text).

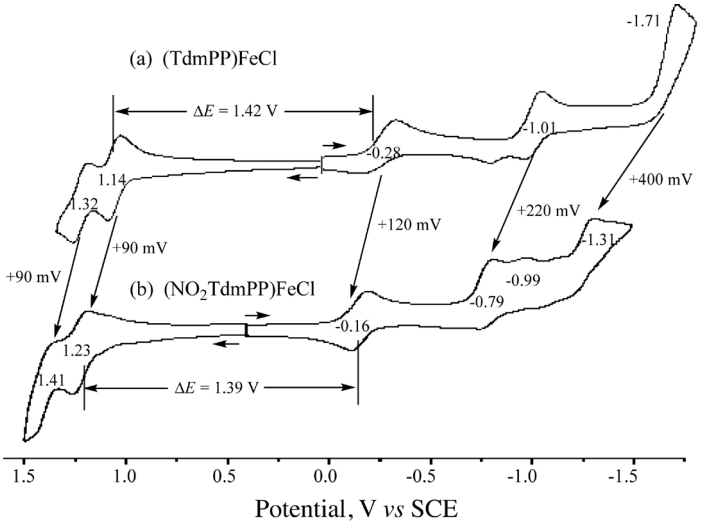

Fig. 2. Cyclic voltammograms of (a) (TdmPP)FeCl **2c** and (b) (NO_2TdmPP)FeCl **2d** in CH_2Cl_2 containing 0.1 M TBAP. Scan rate at 0.10 V/s

(TdmPP)FeCl **2c** which are located at $E_{1/2}$ = -0.28, -1.01 V, 1.14 and 1.32 V in the same solvent (see Fig. 2). Similar positive shifts in potential are also seen for the redox reactions of (NO_2TmPP)FeCl **2b** as compared to (TmPP)FeCl **2a**, with the exact potentials being given in Table 2.

The first reduction of each iron porphyrin, both the nitro and non-nitro derivatives, is reversible and involves a conversion of Fe(III) to Fe(II). This process occurs at -0.18 V for the room temperature reduction of (NO_2TmPP)FeCl **2b** in CH_2Cl_2, 0.1 M TBAP and is labeled as Process I in Fig. 3a. The second room temperature reduction of (NO_2TmPP)FeCl occurs at $E_{1/2}$ = -0.81 V and is labeled as Process II. The first two one-electron reductions of (NO_2TmPP)FeCl involve well-defined peaks with about equal currents and these reactions are followed at more negative potentials by a third reduction peak at E_p = -1.13 V which has a much smaller peak current. This third peak is labeled as Process II' in Fig. 3a. A fourth reduction is located at E_p = -1.29 V (see Table 2) and is not shown in the figure. This peak can be compared to the process at E_p = -1.31 V in Fig. 2 for reduction of compound **2d**.

We previously demonstrated that the first one-electron reduction of β-pyrrole brominated iron porphyrins, (Br_xTPP)FeCl (x = 0–8), results in a mixture of [(Br_xTPP)-$Fe^{II}Cl]^-$ and (Br_xTPP)Fe^{II} [59] and a similar equilibria is proposed to exist between the chloride-bound and non-chloride bound forms of the two electrogenerated Fe(II) nitroporphyrins in CH_2Cl_2. In order to examine this proposed equilibrium, two experiments were carried out, one involving the low temperature electrochemistry of (NO_2TmPP)FeCl in 0.1 M TBAP and the other involving measurements of the same porphyrin at room temperature in solutions containing 0.1 M tetrabutylammonium chloride (TBACl). The electrochemistry of (NO_2TmPP)FeCl under these two solution conditions is illustrated by the cyclic voltammograms in the middle and bottom sections of Fig. 3.

As seen in Fig. 3a, a lowering of the temperature from room temperature to -60 °C results in a decrease in current for the peak labeled as Process II and an increase in that for Process II'. This behavior is consistent with the reduction mechanism shown in Scheme 2 where the initial (NO_2TRPP)Fe^{III}Cl reduction product is assigned as [(NO_2TRPP)$Fe^{II}Cl]^-$ after the addition of one electron (Process I). The electrogenerated Fe(II) porphyrin with an unreduced macrocycle can lose Cl^- to give (NO_2TRPP)Fe^{II} as shown in the scheme and then be further reduced to [(NO_2TRPP)$Fe^{I}]^-$ *via* Process II. Alternatively, the Fe(II) porphyrin with bound Cl^- ion be reduced directly to [(NO_2TRPP)$Fe^{II}Cl]^{2-}$ at a more negative potential (Process II′) before being converted to (NO_2TRPP)Fe^{I} after loss of the axial Cl^- ligand. In this latter process, there would be a transfer of charge from the conjugated macrocycle to the iron center. In either sequences of steps, [(NO_2TRPP)$Fe^{I}]^-$ would be the final product of the overall two electroreductions of (NO_2TRPP)Fe^{III}Cl. The third reduction of the two nitroporphyrins is quasireversible by cyclic voltammetry and this is shown in Fig. 2b for the case of (NO_2TdmPP)FeCl. This one electron addition is assigned as involving a conversion of the iron(I) porphyrin to its iron(I) porphyrin π-anion radical form, as was earlier reported for (TPP)FeCl [59, 61].

The Fe(II) product of the first one-electron reduction contains bound Cl^- and is assigned as [(NO_2TRPP)$Fe^{II}Cl]^-$. This anionic species appears to be stable in solution at room temperature in the absence of an applied potential. Its direct reduction by one electron at more negative potentials leads to a transient doubly reduced Fe(II) porphyrin which also contains axially ligated chloride ion, but this species is rapidly converted to its Fe(I) form upon a loss of Cl^- as shown in Scheme 2. An earlier study of (F_{20}DPP)FeCl suggested a similar electron transfer mechanism for (F_{20}DPP)Fe^{III}Cl which was reduced to [(F_{20}DPP)$Fe^{II}Cl]^{2-}$ prior to the loss of axially bound chloride ion, with generation of an Fe(I) porphyrin as the final two-electron reduction product [60].

Additional proof for assignment of the reactant and product in Process II of Scheme 2 comes from cyclic voltammograms obtained in CH_2Cl_2 solutions containing added chloride ion in the form of TBACl. An example of the cyclic voltammogram under these conditions is shown in Fig. 3b for the case of (NO_2TmPP)FeCl. As seen in this figure, the reduction peak II′ in CH_2Cl_2 containing 0.1 M TBACl is well-defined and has almost the same maximum peak current as for the reduction process I. The cathodic reduction peak for II′ is located at -1.00 V for a scan rate of 0.1 V/s and the anodic reoxidation is located

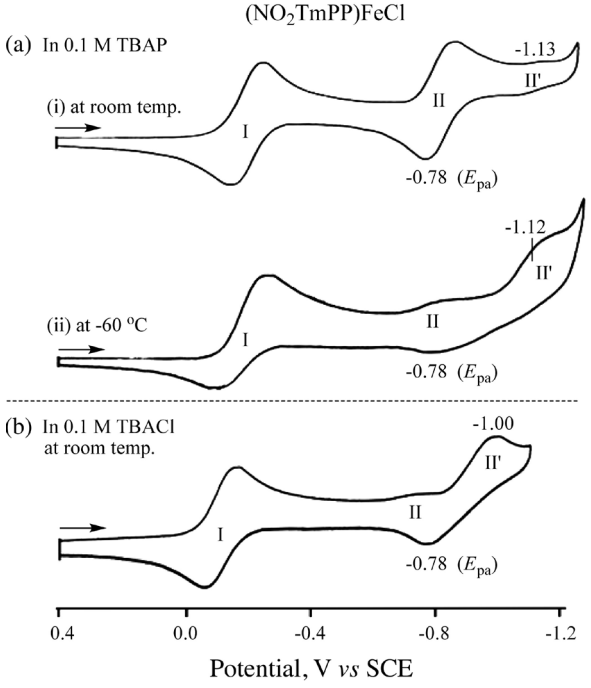

Fig. 3. Cyclic voltammograms showing the reductions of $(NO_2TmPP)FeCl$ **2b** in CH_2Cl_2 (a) containing 0.1 M TBAP at room and low temperature and (b) containing 0.1 M TBACl at room temperature

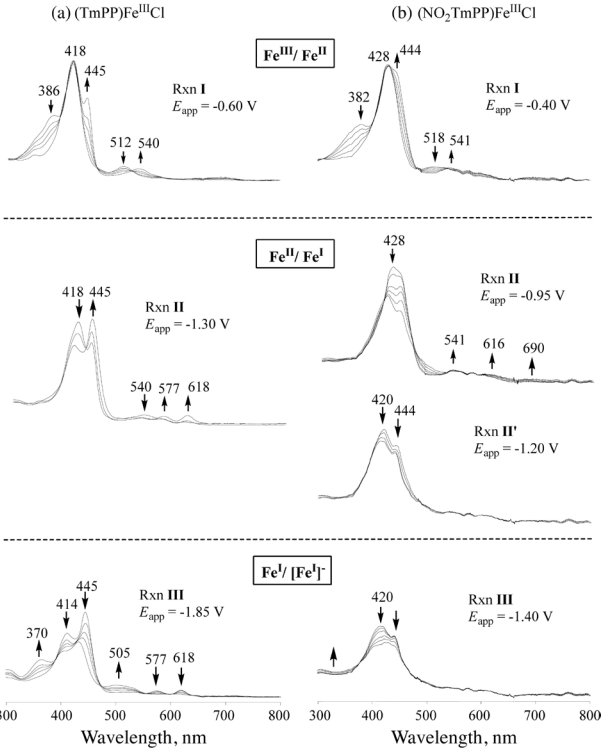

Fig. 4. Thin-layer UV-visible spectral changes of (a) $(TmPP)Fe^{III}Cl$ **2a** and (b) $(NO_2TmPP)Fe^{III}Cl$ **2b** during controlled potential reductions in CH_2Cl_2 containing 0.1 M TBAP

at E_{pa} = -0.78 V. An anodic peak at the same potential is seen for reoxidation of electroreduced $(NO_2TmPP)FeCl$ at room temperature or at -60 °C as seen in Fig. 3.

The investigated iron(II) porphyrins each exhibit a split Soret band between 418 and 446 nm and one Q-band at 540–544 nm (see Table 1). Similar spectral patterns have been reported for other Fe(II) porphyrins in nonaqueous media [59–64].

Quite different UV-visible spectral patterns are seen during the second controlled potential reduction of (TmPP)FeCl and $(NO_2TmPP)FeCl$ in a thin-layer cell (Rxn II in Fig. 4). The reductions of both porphyrins lead ultimatly to an Fe(I) porphyrin as a final product but two different mechanisms are proposed as shown in Scheme 2. A direct reduction of Fe(II) to Fe(I) occurs for (TmPP)FeCl and (TdmPP)FeCl, as is also the case for OEP [65, 66] and TPP complexes [59, 61]. In contrast, the nitro-substituted Fe(II) porphyrins both undergo an initial reduction at the conjugated π-system to give an Fe(II) π-anion radical and this form of the reduced porphyrin is then converted to an Fe(I) porphyrin product after loss of the Cl^- axial ligand.

In a previous study of $[(CN)_4TPP]FeCl$, an equilibrium between an iron(I) porphyrin and an iron(II) porphyrin π-anion radical was proposed, with the iron(II) radical anion assigned as the major contributor to the resonance form of the compound [61]. A similar equilibrium between an Fe(I) porphyrin and an Fe(II) porphyrin π-anion radical was also proposed after the two electroreductions of $(F_{20}DPP)FeCl$ [60]. Both the tetra-cyano porphyrin and the fluorinated dodecaporphyrin contain highly electron-withdrawing substituents, as is also the case for the currently investigated nitroporphyrins.

In summary, the overall electroreduction mechanism of $(NO_2TmPP)FeCl$ and $(NO_2TdmPP)FeCl$ in CH_2Cl_2, 0.1 M TBAP is proposed to occur as shown in Scheme 2. A dissociation of the chloride axial ligand from the electrogenerated Fe(II) porphyrins is favored after a one electron reduction of (TmPP)FeCl and (TdmPP)FeCl in CH_2Cl_2. However, the electron density at the iron(II) center of the porphyrin decreases when an NO_2 group is introduced into the macrocyclic π-ring system as in the case of $(NO_2TmPP)FeCl$ and $(NO_2TdmPP)FeCl$. This results in a strengthening of the Fe–Cl bond for the singly reduced β-nitro substituted porphyrins. The retaining of a chloride axial ligand results in a sufficent shift in electron density at the iron center such that reduction occurs at the macrocycle instead of the metal. Consequently, the second reduction of $(NO_2TmPP)FeCl$ and $(NO_2TdmPP)FeCl$ occurs *via* processes II′ to generate an Fe(II) porphyrin π-anion radical prior to formation of an Fe(I) porphyrin as the ultimate reduction product (see Fig. 3). Further reduction of the Fe(I) porphyrin by one electron yields the Fe(I) π anion radical.

Controlled potential oxidations of each iron porphyrin were also carried out in a thin-layer cell in CH_2Cl_2 containing 0.1 M TBAP and the spectral changes are illustrated in Fig. 5 for $(TmPP)Fe^{III}Cl$ and $(NO_2TmPP)Fe^{III}Cl$.

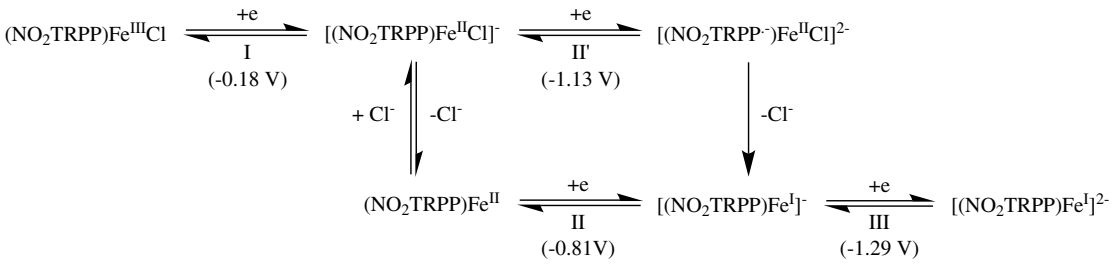

Scheme 2. Proposed reduction mechanism of iron nitroporphyrins in CH_2Cl_2, 0.1 M TBAP, where the potentials in scheme are those for $(NO_2TmPP)FeCl$

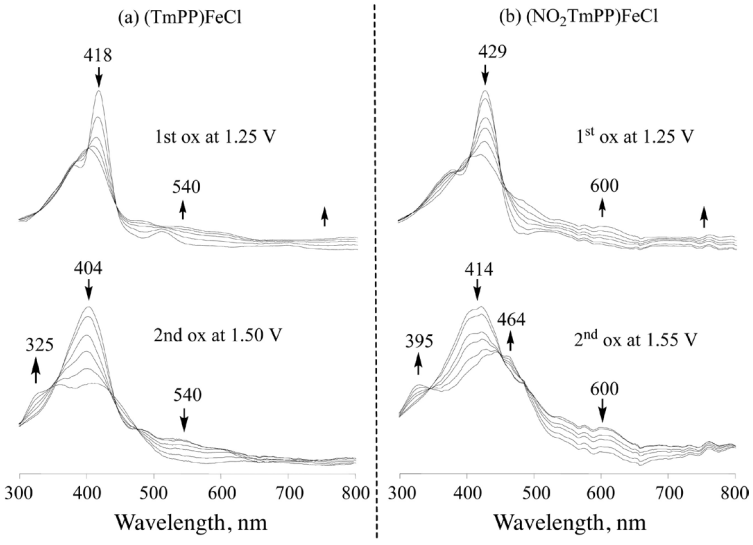

Fig. 5. Thin-layer UV-visible spectral changes of (a) $(TmPP)Fe^{III}Cl$ **2a** and (b) $(NO_2TmPP)Fe^{III}Cl$ **2b** during controlled potential oxidations in CH_2Cl_2 containing 0.1 M TBAP

As seen in the figure, the Soret band continuously decreases in intensity upon the first and second oxidations for each compound, thus indicating that Fe(III) π-cation radical and dianions are formed as two electrons are stepwise removed from the porphyrin macrocycle.

Manganese porphyrins. The electrochemical behavior of the two β-nitro substituted manganese porphyrins differs from what is seen for the unsubstituted compounds, (TmPP)MnCl and (TdmPP)MnCl, in nonaqueous media. The half-wave and peak potentials of each Mn(III) porphyrin are given in Table 2 while examples of the cyclic voltammograms of (TmPP)MnCl and $(NO_2TmPP)MnCl$ in CH_2Cl_2 containing 0.1 M TBAP are shown in Fig. 6.

The highly electron-withdrawing nitro group on $(NO_2TmPP)MnCl$ and $(NO_2TdmPP)MnCl$ leads to a substantial positive shift in redox potentials, with three reductions being observed for the β-NO_2 substituted compounds in CH_2Cl_2 as compared to the parent compounds, (TmPP)MnCl and (TdmPP)MnCl which exhibit only two reductions under the same solution conditions (Table 2). These results are consistent with what was previously reported for other β-NO_2 substituted manganese porphyrins [33].

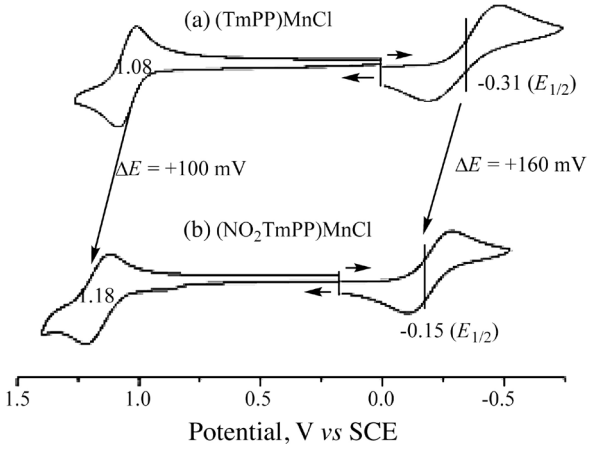

Fig. 6. Cyclic voltammograms shown the first reduction and first oxidation of (a) (TmPP)MnCl **3a** and (b) (NO_2TmPP)-MnCl **3b** in CH_2Cl_2 containing 0.1 M TBAP

Each current investigated manganese(III) porphyrin in CH_2Cl_2 exhibits a split Soret band, located between 379 and 490 nm. There are also two Q-bands at 581–594 and 616–640 nm (Table 1). Significant spectral changes

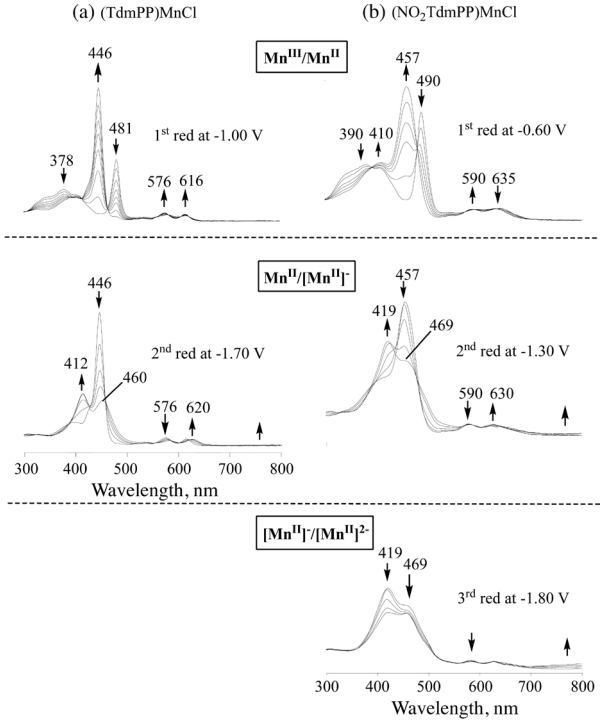

Fig. 7. Thin-layer UV-visible spectral changes of (a) (TdmPP)MnCl **3c** and (b) (NO_2TdmPP)MnCl **3d** during the controlled potential reductions in CH_2Cl_2 containing 0.1 M TBAP

are observed during the controlled potential reduction in CH_2Cl_2 containing 0.1 M TBAP, with examples being given in Fig. 7 for (TdmPP)MnCl and (NO_2TdmPP)MnCl. The spectrum of the singly reduced Mn(III) porphyrins exhibits an intense Soret band at 445–447 nm, a shoulder at 403–410 nm and two visible bands between 576–590 and 616–650 nm (Table 1). This electrode reduction has generally been assigned as a Mn^{III}/Mn^{II} conversion [63, 67]. The reductions which occur at more negative potentials are assigned to porphyrin ring-centered electron transfer processes to give Mn(II) π-anion radicals and dianions.

Figure 8 illustrates of the spectral changes which occur for (TdmPP)MnCl and (NO_2TdmPP)MnCl during controlled potential oxidation in CH_2Cl_2 containing 0.1 M TBAP. Similar spectral changes are seen for these two compounds upon the first and second one-electron abstractions, suggesting that the NO_2 substituted and unsubstituted porphyrins both follow the same electron transfer mechanism under the given experimental conditions. As seen in Fig. 8, the Soret band at 481 nm for (TdmPP)MnCl **3c** and at 490 nm for (NO_2TdmPP)MnCl **3d** both decrease in intensity while a broad visible band grows in at 660 nm (**3c**) or 695 nm (**3d**). Mn(III) π-cation radicals are generated during the first one-electron oxidation of these compounds and the second oxidation is then assigned to the formation of a Mn(III) dication in CH_2Cl_2.

Factors affecting the magnitude of the NO_2 substituent effect. As mentioned earlier, the magnitude of the NO_2 substituent effect on redox potentials for reduction or oxidation of a nitro-porphyrin will depend not only on the specific placement of the nitro substituent on the compound but also on the site of electron transfer (oxidation or reduction, metal or macrocycle), and the nature of the central metal ion. This is seen by the data in Table 3 which compares substituent effects for adding a single nitro group directly onto the *meso*-position of a porphyrin with that of a porphyrin or corrole containing one β-pyrrole substituted nitro group.

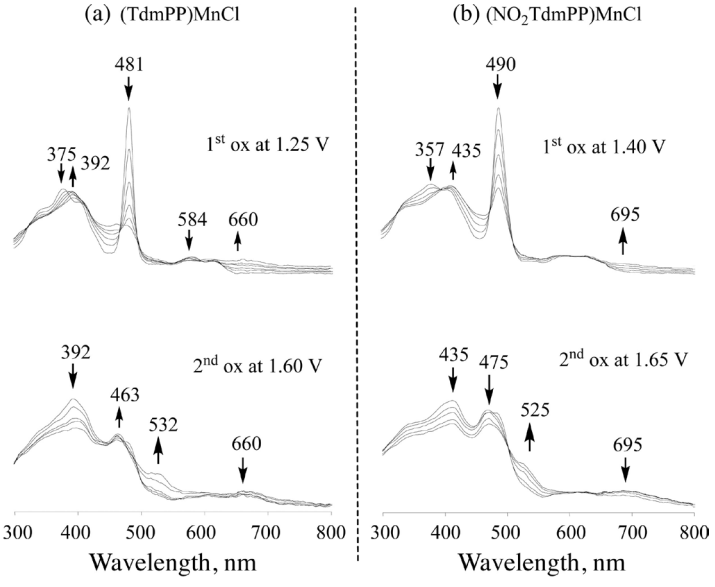

Fig. 8. Thin-layer UV-visible spectral changes of (a) (TmPP)MnCl **3c** and (b) (NO_2TmPP)MnCl **3d** during the controlled potential oxidations in CH_2Cl_2 containing 0.1 M TBAP

Table 3. Comparison of the first reduction and oxidation potentials for the four types of NO_2-substituted porphyrins

Type of Cpd	Macrocycle[a]	M	#NO_2	First oxidation		First reduction		Reference
				$E_{1/2}$, V	ΔE, mV[b]	$E_{1/2}$, V	ΔE, mV[b]	
meso-NO_2 porphyrin	OEP	2H	0	1.04		-1.19		
			1	1.23	**190**	-0.85	**340**	39
		Zn(II)	0	0.87		-1.47		
			1	1.01	**140**	-1.02	**450**	39
		Cu(II)	0	0.81		-1.37		
			1	1.04	**130**	-0.84	**530**	40
β-NO_2 porphyrin	TPP	2H	0	1.03		-1.01		
			1	1.15	**120**	-0.72	**290**	23
		Cu(II)	0	0.69		-1.64		
			1	0.78	**90**	-1.27	**370**	23
		Zn(II)	0	0.57		-1.67		
			1	0.70	**130**	-1.29	**380**	23
	TmPP	2H	0	0.95		-1.19		
			1	1.06	**110**	-0.81	**280**	*tw*
		Fe(III)	0	1.07		-0.27		
			1	1.14	**70**	-0.18	**90**	*tw*
		Mn(III)	0	1.08		-0.31		
			1	1.18	**100**	-0.15	**160**	*tw*
	TdmPP	2H	0	1.02		-1.12		
			1	1.15	**130**	-0.83	**290**	*tw*
		Fe(III)	0	1.14		-0.28		*tw*
			1	1.26	**90**	-0.16	**120**	
		Mn(III)	0	1.14		-0.29		
			1	1.26	**120**	-0.10	**190**	*tw*
β-NO_2 corrole	TMPCor	Fe(III)	0	0.82		-0.35		
			1	1.01	**190**	-0.16	**190**	55
	TNPCor	Fe(III)	0	0.97		-0.14		55
			1	1.18	**210**	-0.05	**190**	
	T*t*BuPCor	Ag(III)	0	-0.03		-0.79		
			1	1.21	**240**	-0.54	**250**	57
		Cu(III)	0	0.71		-0.17		
			1	1.90	**190**	-0.00	**170**	56

[a] TMPCor and TNPCor are the trianions of the tri-methoxylphenylcorrole and tri-nitrophenylcorrole, respectively, T*t*BuPCor is the trianions of the tri-butylphenylcorrole and the data measured in pyridine for Ag(III) corroles containing 0.1 M TBAP. [b] $\Delta E_{1/2}$ = the potential difference between $E_{1/2}$ for the reduction or oxidations of the nitrocorrole and the parent corrole without the nitro group.

The largest substituent effect upon reduction is seen for the *meso*-substituted compounds, as shown in Table 3 for the free-base, Zn(II) and Cu(II) complexes of substituted OEP, where $\Delta E_{1/2}$ varies between 340 and 530 mV [39, 40]. In contrast, the β-pyrrole substituted TPP compounds with 2H, Zn(II) or Cu(II) centers show $\Delta E_{1/2}$ values which range between 290 and 380 mV [23].

The shift in potential between the free-base nitro and free-base non-nitro substituted TPP complexes was reported to be 290 mV in CH_2Cl_2 [23] and a similar shift of 280 and 290 mV is seen for the two currently investigated free-base porphyrins with OCH_3 or CH_3 substituents. In contrast, the Mn(III)/Mn(II) reaction of the currently studied compounds has a smaller nitro substituent effect of 160 and 190 mV, and this shift in potential is decreased even further in the case of the Fe(III)/Fe(II) reactions, where a $\Delta E_{1/2}$ of 90 and 120 mV shift is seen for the two investigated porphyrins.

The above trends in nitro group substituent effects as a function of changes in the type of central metal ion are

consistent with what has been observed for other redox-active and redox-inactive metalloporphyrins [67], but it varies substantially from what occurs in the case of the β-pyrrole substituted corroles. This is evident from the data in Table 3, where the metal-centered reduction of the Cu(III), Fe(III) and Ag(III) derivatives to their lower M(II) oxidation state has a larger substituent effect ranging from 170 to 250 mV [55–57]. This increased value of $\Delta E_{1/2}$ for the the metal-centered reduction of the corroles is consistent with a larger interaction existing between the corrole central metal ion and the conjugated macrocycle than in the case of the porphyrins where the metal and the macrocycle orbitals are better separated.

Finally, it should be pointed out that the nitro-substituent effects on oxidation of porphyrins are substantially smaller than those for reduction but this is not what occurs for Fe(III), Ag(III) and Cu(III) corroles where the oxidations and reductions are similarly effected by the nitro group and may in fact be slightly larger for oxidation, as seen in Table 3.

CONCLUSION

In summary, the electron-withdrawing NO_2 substituent on the β-pyrrole position of (NO_2TmPP)M and (NO_2TdmPP)M leads to a much easier reduction and a slightly harder oxidation as compared to the unsubstituted parent porphyrins. There is also a red-shift in the UV-visible spectra of the compounds having the nitro group. The unsubstituted Fe(III) porphyrin favors formation of an Fe(I) porphyrin upon reduction in CH_2Cl_2 but reduction of the β-pyrrole NO_2-substituted porphyrin leads to an Fe(II) porphyrin π-anion radical under the same experimental conditions. The addition of one NO_2 group to the β-pyrrole position of the porphyrin has a larger effect on the redox potentials than for addition to the *meso*-phenyl rings of the compound. The observed shifts in reduction/oxidation potentials for addition of an NO_2 group to the β-pyrrole position of the currently investigated porphyrins is similar to that which was earlier reported for reduction and oxidation of β-pyrrole substituted triphenylcorroles containing the same central metal ions.

Acknowledgements

We gratefully acknowledge supports from the Natural Science Foundation of China (No. 21071067, 21001054), Postdoctoral Science Foundation of China (2012M511203) and Jiangsu Province (1102126C), and the Robert A. Welch Foundation (K.M.K., Grant E-680).

REFERENCES

1. Sessler JL and Weghorn SJ. *Expanded, Contracted, and Isomeric Porphyrins*, Elsevier: Oxford, 1997.
2. *The Porphyrin Handbook*, Vol. 6, Kadish KM, Smith KM and Guilard R. (Eds.) Academic Press: San Diego, CA, 2000.
3. *Handbook of Porphyrin Science: With Applications to Chemistry, Physics, Materials Science, Engineering, Biology and Medicine*, Vol. 12, Kadish KM, Smith KM and Guilard R. (Eds.) World Scientific: Hackensack, NJ, 2010.
4. Bhyrappa P and Purushothaman B. *J. Chem. Soc., Perkin Trans. 2*, 2001; 238–242.
5. Dahal S, Krishnan V and Nethaji M. *Proc. Indian Acad. Sci. (Chem. Sci.)* 1998; **110**: 37–52.
6. Bartoli J-F, Mouries-Mansuy V, Barch-Ozette KL, Palacio M, Battioni P and Mansuy D. *Chem. Commun.* 2000; 827–828.
7. Wyrębeka P and Ostrowski S. *J. Porphyrins Phthalocyanines* 2007; **11**: 822–828.
8. Ostrowski S and Grzyb S. *Tetrahedron Letters* 2012; **53**: 6355–6357.
9. Horn S, Dahms K and Senge MO. *J. Porphyrins Phthalocyanines* 2008; **12**: 1053–1077.
10. Chen ZP, Guo ZQ, Huang QM and Wu XJ. *Wuhan Univ. J. Nat. Sci.* 2002; **7**: 345–349.
11. Terekhov SN, Sinyakova GN, Lobkoa EE, Pierrette B, Turpinc PY and Chirvony VS. *J. Porphyrins Phthalocyanines* 2007; **11**: 682–690.
12. Prasath R, Butcher RJ and Bhavana P. *Spectrochimica Acta Part A* 2012; **87**: 258–264.
13. Siri O, Jaquinod L and Smith KM. *Tetrahedron Letters* 2000; **41**: 3583–3587.
14. Palacio M, Mansuy-Mouries V, Loire G, Barch-Ozette KL, Leduc P, Barkigia KM, Fajer J, Battioni P and Mansuy D. *Chem. Commun.* 2000; 1907–1908.
15. Kadish KM, Ou ZP, Tan XY, Boschi T, Monti D, Fares V and Tagliatesta P. *J. Chem. Soc*., *Dalton Trans*. 1999; 1595–1601.
16. Vicente MGH, Neves MGPMS and Cavaleiro JAS. *Tetrahedron Letters* 1996; **37**: 61–262.
17. Girolami GS, Gorlin PA and Suslick KS. *Inorg. Chem.* 1994; **33**: 626–621.
18. Sibilia SA, Czernuszewicz RS, Crossley MJ and Spiro TG. *Inorg. Chem*. 1997; **36**: 6450–6453.
19. Crossley MJ, King LG and Simpson JL. *J. Chem. Soc., Perkin Trans. 1: Org. Bio-Org. Chem*. 1997; 3087–3096.
20. Crossley MJ and King LG. *J. Chem. Soc., Perkin Trans. 1: Org. Bio-Org. Chem*. 1996; 1251–1260.
21. Crossley MJ, Harding MM and Tansey CW. *J. Org. Chem*. 1994; **59**: 4433–4437.
22. Crossley MJ and King LG. *J. Org. Chem*. 1993; **58**; 4370–4375.
23. Binstead RA, Crossley MJ and Hush NS. *Inorg. Chem*. 1991; **30**: 1259–1264.
24. Crossley MJ, Gosper JJ and King LG. *Tetrahedron Letters* 1988; **29**: 1597–1600.
25. Crossley MJ, Gosper JJ and Wilson MG. *J. Chem. Soc., Chem. Comm*. 1985; 1798–1799.
26. Catalano MM, Crossley MJ and King LG. *J. Chem. Soc., Chem. Comm*. 1984; 1537–1538.

27. Baldwin JE, Crossley MJ and DeBernardis J. *Tetrahedron* 1982; **38**: 685–692.
28. Crossley MJ, Sheehan CS, Khoury T, Reimers JR and Sintic PJ. *New J. Chem*. 2008; **32**: 340–352.
29. Takahashi K, Hase S, Komura T, Imanaga H and Ohno O. *Bull. Chem. Soc. Jap.* 1992; **65**: 1475–1481.
30. Hu J, Pavel I, Moigno D, Wumaier M, Kiefer W, Chen Z, Ye Y, Wu Q, Huang Q, Chen S, Niu F and Gu Y. *Spectrochimi. Acta Part A* 2003; **59**: 1929–1935.
31. Ou ZP, Kadish KM, E W, Shao JG, Sintic PJ, Ohkubo K, Fukuzumi S and Crossley MJ. *Inorg. Chem.* 2004; **43**: 2078–2086.
32. Rao TA and Maiya BG. *Polyhedron* 1994; **13**: 1863–1873.
33. Ozette K, Battioni P, Leduc P, Bartoli J-F and Mansuy D. *Inorg. Chim. Acta* 1998; **272**: 4–6.
34. Hombrecher HK, Gherdan VM, Ohm S, Cavaleiro JAS, Neves MDGPMS and Condesso MDF. *Tetrahedron* 1993; **49**: 8569–8578.
35. Kadish KM, Ou ZP, Tan XY, Boschi T, Monti VF and Tagliatesta P. *J. Chem. Soc., Dalton. Trans*. 1999; **10**: 1595–1602.
36. Martelli C, Canning J, Khoury T, Skivesen N, Kristensen M, Huyang G, Jensen P, Neto C, Sum TJ, Hovgaard MB, Gibson BC and Crossley MJ. *J. Mat. Chem*. 2010; **20**: 2310–2316.
37. Crossley MJ, King LG, Pyke SM and Tansey CW. *J. Porphyrins Phthalocyanines* 2002; **6**: 685–694.
38. Wickramasinghe A, Jaquinod L, Nurco DJ and Smith KM. *Tetrahedron* 2001; **57**: 4261–4269.
39. Gong LG and Dolphin D. *Can. J. Chem*. 1985; **63**: 401–405.
40. Wu GZ, Leung HK and Gan WX. *Tetrahedron* 1990; **46**: 3233–3244.
41. Fadda AA, El-Mekawy RE, El-Shafei AI and Freeman H. *Archiv der Pharmazie* 2013; **346**: 53–61.
42. Frixa C, Mahon MF, Thompson AS and Threadgill MD. *Org. Biomol. Chem*. 2003; **1**: 306–317.
43. Sun ZC, She YB, Zhou Y, Song XF and Li K. *Molecules* 2011; **16**: 2960–2970.
44. Kleij AW, Kuil M, Tooke DM, Spek AL and Reek JNH. *Inorg. Chem.* 2005; **44**: 7696–7698.
45. Vermathen M, Louie EA, Chodosh AB, Ried S and Simonis U. *Langmuir* 2000; **16**: 210–221.
46. Yoshimura T. *Bull. Chem. Soc. Japn*. 1991; **64**: 2819–2821.
47. Kadish KM, Lin XQ, Ding JQ, Wu YT and Araullo C. *Inorg. Chem*. 1986; **25**: 3236–3242.
48. Yap BCM, Simpkins GL, Collyer CA, Hunter N and Crossley MJ. *Org. Biomol. Chem*. 2009; **7**: 2855–2863.
49. Sintic PJ, E W, Ou ZP, Shao JG, McDonald JA, Cai ZL, Kadish KM, Crossley MJ and Reimers JR. *Phys. Chem. Chem. Phys.* 2008; **10**: 515–527.
50. Crossley MJ, Sintic PJ, Hutchison JA and Ghiggino KP. *Org. Biomol. Chem*. 2005; **3**: 852–865.
51. Kadish KM, E W, Sintic PJ, Ou ZP, Shao JG, Ohkubo K, Fukuzumi S, Govenlock LJ, McDonald JA, Try AC, Cai ZL, Reimers JR and Crossley MJ. *J. Phys. Chem. B* 2007; **111**: 8762–8774.
52. Kadish KM, Van Caemelbecke E and Royal G. In *The Porphyrin Handbook*, Vol. 8, Kadish KM, Smith KM and Guilard R. (Eds.) Academic Press: New York, 2000; Chapter 55, pp 1–144.
53. (a) Shi TS, Sun HR, Cao XZ and Tao JZ. *Chem. J. Chinese Univ*. 1994; **15**: 966–969. b) Tao JZ, Sun HR, Shi TS and Cao XZ. *Chem. J. Chinese Univ*. 1994; **15**: 1657–1661.
54. Stefanelli M, Pomarico G, Tortora L, Nardis S, Fronczek FR, McCandless GT, Smith KM, Manowong M, Fang Y, Chen P, Kadish KM, Rosa A, Ricciardi G and Paolesse R. *Inorg. Chem*. 2012; **51**: 6828–6942.
55. Nardis S, Stefanelli M, Mohite P, Pomarico G, Tortora L, Manowong M, Chen P, Kadish KM, Fronczek FR, McCandless GT, Smith KM and Paolesse R. *Inorg. Chem*. 2012; **51**: 3910–3920.
56. Stefanelli M, Mandoj F, Mastroianni M, Nardis S, Mohite P, Fronczek FR, Smith KM, Kadish KM, Xiao X, Ou ZP, Chen P and Paolesse R. *Inorg. Chem*. 2011; **50**: 8281–8292.
57. Stefanelli M, Shen J, Zhu WH, Mastroianni M, Mandoj F, Nardis S, Ou ZP, Kadish KM, Fronczek FR, Smith KM and Paolesse R. *Inorg. Chem*. 2009; **48**: 6879–6887.
58. Giraudeau A, Callot HJ, Jordan J, Ezhar I and Gross M. *J. Am. Chem. Soc.* 1979; **101**: 3857–3862.
59. Tagliatesta P, Li J, Autret M, Van Caemelbecke E, Villard A, D'Souza F and Kadish KM. *Inorg. Chem*. 1996; **35**: 5570–5576.
60. Kadish KM, Van Caemelbecke E, D'Souza F, Lin M, Nurco DJ, Medforth CJ, Forsyth TP, Krattinger B, Smith KM, Fukuzumi S, Nakanishi I and Shelnutt JA. *Inorg. Chem*. 1999; **38**: 2188–2198.
61. Kadish KM, Boisselier–Cocolios B, Simonet B, Chang D, Ledon H and Cocolios P. *Inorg. Chem.* 1985; **24**: 2148–2156.
62. Pellegrino J, Hubner R, Doctorovich F and Kaim W. *Chem. Eur. J.* 2011; **11**: 7868–7874.
63. Kadish KM, Shao JG, Ou ZP, Zhan RQ, Burdet F, Barbe J-M, Gros CP and Guilard R. *Inorg. Chem*. 2005; **44**: 9023–9038.
64. Kadish KM, Van Caemelbecke E, D'Souza F, Medforth CJ, Smith KM, Tabard A and Guilard R. *Inorg. Chem*. 1995; **34**: 2984–2989.
65. Teraoka J, Hashimoto S, Sugimoto H, Mori M and Kitagawa T. *J. Am. Chem. Soc.* 1987; **109**: 180–184.
66. Wei ZC and Ryan MD. *Inorg. Chem*. 2010; **49**: 6948–6954.
67. Kelly SL and Kadish KM. *Inorg. Chem*. 1982; **21**: 3631–3639.